Application Of Multiphoton steady state and lifetime imaging to mapping of tumour vascular architecture *in vivo*

S. M. Ameer-Beg[*a], P. R. Barber [a], R. J. Hodgkiss [a], R. J. Locke [a], R.G. Newman, G. M. Tozer [b], B. Vojnovic [a], J. Wilson [b]
[a]Advanced Technology Development Group; [b]Tumour Microcirculation Group, Gray Cancer Institute

ABSTRACT

Recent interest in vascular targeting and anti-angiogenic drug treatments for cancer has stimulated fundamental research regarding the modes of action of these drugs as well as studies of the development and re-modelling of the vascular network following treatment. Multiphoton fluorescence microscopy is employed for *in vivo* mapping of three-dimensional blood vessel distribution in tumours grown in rodent dorsal skin-flap window chamber preparations. Accurate visualisation of the vasculature in three-dimensions allows us to perform dynamic experiments in thick biological specimens *in vivo*. Examples of *in vivo* imaging of tumour vasculature are given and compared to normal tissue vasculature. The dynamic responses of blood vessels to treatment with the vascular targeting drug combretastatin A4-P are presented and discussed.
The implementation of time-domain imaging by reversed stop-start time-correlated single photon counting (RSS-TCSPC) is discussed as a method for feature extraction in the presence of exogenous and endogenous fluorophores. In particular, the segmentation of the vascular network is demonstrated. Additional contrast, indicative of probe environmental factors, may also be realised. We present examples of *in vivo* lifetime imaging as a method to elucidate the physiological processes of the tumour microenvironment.

Keywords: multi-photon, *in vivo,* vasculature, combretastatin-A4-phosphate, intra-vital microscopy, blood vessel, TCSPC, time-resolved.

1. INTRODUCTION

Recently, the development and subsequent commercialisation of solid-state femtosecond laser sources has enabled many advanced spectroscopic techniques to become standard tools for the investigation of fundamental processes in physics, chemistry and biology[1]. One such application, which has shown considerable promise in the area of biological imaging, is multiphoton microscopy (MPM)[2]. The particular advantage of MP imaging is conferred by the use of intense near-infrared (NIR) light to induce non-linear absorption in a probe fluorophore. The intensity dependence of the non-linear absorption confines the excitation to the focal plane of the imaging lens. This inherent sectioning capability allows the collection of 3-dimensional data without the use of a confocal aperture, since fluorescence is generated only in the focal volume allowing simplified detection systems to be employed[3]. Since the NIR is inherently scattered to a lesser degree than the visible (Rayleigh scattering $\propto \lambda^{-4}$) and linear absorption of the NIR is minimal for most biological applications, thick (< 500 μm) samples may be imaged[4]. Photobleaching and photodamage are also greatly reduced due to the confinement of excitation to the focal volume[5].

Current technological limitations restrict the application of *in vivo* MPM to readily accessible sites such as the skin[6], the eye[7] and to animal models such as the skinfold[8] or cranial[9] window chamber. Application of the technique to window chamber models of tumour-bearing rodents shows particular promise as an adjunct to established techniques such as intra-vital microscopy and conventional histology. The advantage lies in the three-dimensional resolving power of MPM at depth within the model for determination of structure and function. In addition, experiments to follow tumour development, angiogenesis, treatment and vascular remodelling, as a result, are possible with multiple imaging time-points without compromising the model.

[*] Ameer-beg@gci.ac.uk; phone (+44) 1923 82861; fax (+44) 1923 835210; http://www.gci.ac.uk; Advanced Technology Development Group, Gray Cancer Institute, P.O. Box 100, Mount Vernon Hospital, Northwood, Middlesex, UK HA6 2JR;

The role of blood flow and oxygenation is of crucial importance in the treatment of cancer. In particular, the delivery of nutrients and oxygen via an, often, aberrant vascular network in tumours, affects both growth and the delivery and efficacy of drug treatments. Angiogenic processes in tumours lead to a relatively chaotic blood supply in comparison to normal tissue and consequently blood flow distribution is heterogeneous. This poses a number of problems in terms of treatment, such as the in-homogeneity of drug delivery and the well-known resistance of hypoxic regions of tumours to radiotherapy[10]. The degree of tortuosity and heterogeneity of the tumour vasculature is site and tumour specific and vascular density in tumours has been shown to be predictive for outcome in radiotherapy[11]. Treatments which specifically target the tumour vasculature, show promise as adjuncts to chemo- and radiotherapy. In the present study, the tubulin-binding agent, Combretastatin-A-4-P (CA-4-P) was used as a model drug, which causes an extensive and rapid shut-down of the established tumour vasculature, leading to tumour cell necrosis[12]. Recent studies have demonstrated the applicability of MPM to the study of blood vessel morphology and indeed to the *in vivo* measurement of processes such as angiogenesis, gene expression, invasion and metastases[8,13,14]. In this instance, we demonstrate the mapping of vessel architectures in the window chamber and the ability to map dynamic changes in vessel permeability and structure in response to drug treatment.

Dynamic changes in tumour vasculature are now routinely studied in our laboratory using tumours grown in a rodent dorsal skin flap 'window chamber' of ~0.2-0.5 mm thickness, allowing optical access to tumours and normal tissues *in vivo*. Conventional trans-illumination and fluorescence imaging of such preparations yields valuable information in the focal plane, although the presence (or absence) of out-of-plane objects can lead to ambiguity in determinations of such parameters as inter-vessel distance, branching ratios and leakage of fluorescent markers. Accurate determination of the complete three-dimensional vascular matrix is therefore desirable. The applicability of steady-state MPM to the determination of the complex and often highly heterogeneous three-dimensional tumour vasculature, is therefore primarily limited by scattering, pulse front distortions due to out of plane obstructions and the presence of species with absorption in either the NIR or at the fluorophore emission wavelength. To this end, we present fluorescence lifetime imaging with picosecond time-resolution to provide intensity independent means of contrast for segmentation of the tumour vasculature and for determination of molecular species, to our knowledge, for the first time in tumours *in vivo*.

2. METHODOLOGY

2.1 Multi-photon imaging

Microscopy was performed with a multiphoton microscope system, based on a modified Bio-Rad MRC 1024MP workstation, comprising a solid-state-pumped (10 W Millennia X, Nd:YVO_4, Spectra-Physics), self-mode-locked Ti:Sapphire (Tsunami, Spectra-Physics) laser system, afocal scan-head, confocal detectors and an inverted microscope (Nikon TE200). Enhanced detection of the scattered component of the emitted (fluorescence) photons is afforded by the use of three, in-house developed, non-descanned detectors, situated in the re-projected stationary plane (re-imaged objective back aperture). Fluorescence lifetime imaging capability has been incorporated into the external detector system in a similar manner as reported by Becker *et al*.[15], with addition of photomultiplier tubes with fast single-photon response (Hamamatsu R7401-P), 1 GHz bandwidth amplifier stage and time-correlated single photon counting electronics (Becker & Hickl, SPC 700). Time-resolution of the order of 120 ps is obtained with this arrangement determined by the instrumental response, allowing accurate determination of fluorophore lifetime for the range 0.5-5 ns.

Due to geometrical constraints of the animal models, long working distance objectives must be used and, unless otherwise stated, a 10x Nikon Plan Fluor objective was used (16 mm WD, 0.3 NA) for *in vivo* imaging.

2.2 Dorsal skinfold window chambers

Early generation transplants of the P22 rat carcinosarcoma were grown in transparent window chambers, surgically implanted into the fascial layer of a dorsal skin flap of male BD9 rats[16,17]. Animals weighed 150-200 g at the time of surgery. Multiphoton microscopy was carried out 7 to 14 days following surgery, when tumours measured 2-5 mm in diameter. Tumours, 200 to 500 µm thick, were observed from the surface adjacent to the fascial layer. For *in vivo* imaging, a specially adapted microscope stage allows mounting and positioning of the window chamber above the microscope objective. Prior to imaging the rats were anaesthetised with Hypnorm and midazolam[18] and body temperature was regulated using a thermostatically-controlled heating pad with rectal temperature sensing. For imaging of the blood vessel architecture, a 70 kD anionic dextran conjugated with either Cascade Blue™ or FITC (Molecular Probes) was injected intravenously as a blood pool contrast agent. This dextran appears to be well-tolerated *in vivo* and clearly delineated blood vessels without significant extra-vasation into the surrounding tumour tissue throughout the

period of observation (maximum 4 hours). Investigation of extra-vasation of proteins for measurements of vessel permeability were performed with bovine serum albumin conjugated to FITC (Sigma). Excitation of both Cascade Blue™ and FITC fluorescence was possible using two-photon absorption at 800 nm and isolated from background auto-fluorescence due to endogenous fluorophores using 455 nm and 540 nm filters (30 nm bandpass) respectively. In order to observe dynamic changes in tumour vasculature over a period of 1-4 hours, CA-4-P was given by intra-peritoneal administration (30 mg kg^{-1}).

3. RESULTS AND DISCUSSION

3.1 *Ex vivo* vascular imaging

Vascular networks and other structures have been mapped at depth in several normal rat tissues *ex vivo* e.g. gut (Fig. 1), skin, kidney and brain. In gut (Fig. 1c) and skin, thin auto-fluorescent layers have been observed but, generally, it is necessary to use a fluorescent contrast agent to enable specific structures to be imaged, such as the 70kD FITC-dextran, used in this example to highlight the vasculature. The tissue was excised and imaged two hours after i.v. administration of the contrast agent. Imaging was with a 20x, 0.75 Nikon S Fluor objective to allow penetration to a depth of ~ 200 μm. The highly-organised vasculature is arranged in distinct patterns at different depths within the tissue, reflecting the varying architecture and function of the different layers.

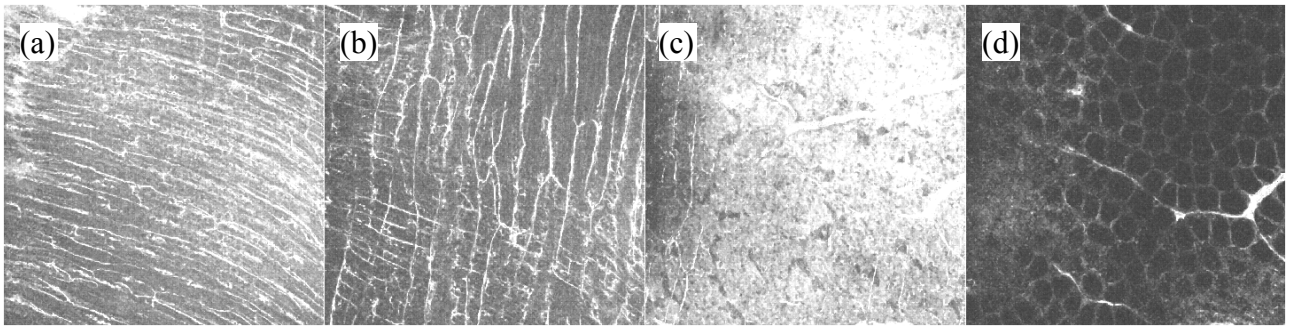

Fig. 1. A typical set of multiphoton images of vasculature at different depths in jejunum of BD9 rat; a) Blood vessels between muscle fibres of the outer longitudinal layer; b) Blood vessels between muscle fibres of the inner circular layer; c) Blood vessels in sub-mucosal layer; d) Blood vessels in the mucosal capillary plexus.

3.2 Quantitative imaging of tumour vasculature

Quantitative analysis of the vasculature is essential if we are to characterise the architecture of the tumours for mathematical analysis and modelling for physiology. With the aid of software written at the GCI we are able to manually delineate the 3d vascular structure from images taken of window chamber preparations of tumours growing in both rats and mice. This is a vital step towards the collection of quantitative data to characterise the vascular architecture and then to compare architectures produced by differing tumour types. We have developed software (Trace3D) that allows the manual delineation of the vascular architecture through the tracing of lines and nodes onto the orthogonal projections of the 3d image. Fig. 2a shows a screen-shot of the software in use, where the right-hand panel shows the vessels traced so far overlaid onto the orthogonal projections of a HT29 human colorectal tumour xenographed into mice.

The initial collection of statistics has been aimed at vessel length as defined as the distance between branching (node) points. This is trivial to calculate once the vector representation of the vessels are obtained. Fig. 1b shows a histogram of vessel lengths from the HT29 tumour xenographed into mice.

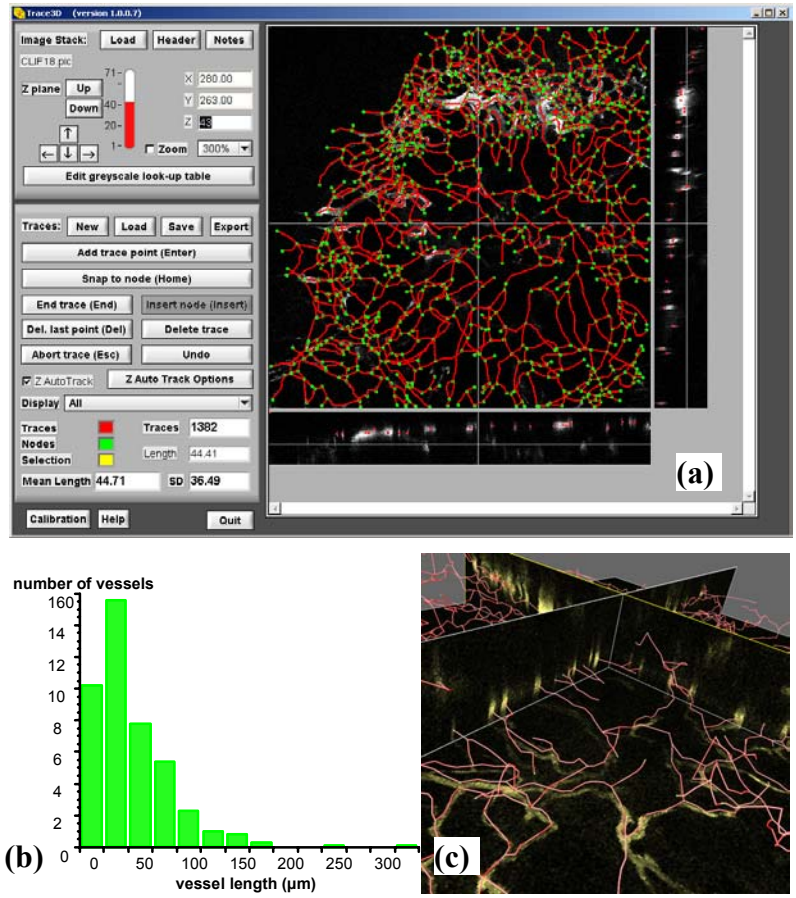

Fig. 2: Mapping the tumour vasculature; a) Screenshot of Trace3D; b) Histogram of vessel lengths for HT29 human colorectal tumour xenograph; c) Rendering of the tumour vessels with map overlay.

Validation of the delineated vascular structure is currently performed by eye. This task is made more simple and reliable through the use of 3d volume rendering software. Several software packages are commercially available that allow volume renders of 3d images to be visualized. One such package, Imaris/Surpass (Bitplane AG, Switzerland), also allows the simultaneous visualisation of vector-based objects. To make use of this the Trace3D software also has the ability to export the delineated vascular tree in a virtual reality model language (VRML) script. This is accepted by Imaris/Surpass to allow the simultaneous and real-time, visualization and exploration of the original volumetric data overlaid with the delineated architecture as shown in Figure 1c.

3.3 Qualitative effect of combretastatin A4-P on the tumour vasculature

Tumour vasculature has been mapped periodically after administration of CA-4-P (30 mg kg^{-1}) to BD9 rats bearing P22 rat carcinosarcoma enabling us to visualise the dynamic effect of the drug on the vasculature at depth in a tumour over a period of 4 hours. We observe rapid changes in the permeability of the vasculature within one hour of administration (Fig. 3). The result suggests that vessels remain, but that extra-vasation of the dye has occurred and appears as an increase in apparent background signal or loss of contrast. We also observed changes in the total fluorescence in the blood vessels, and this can be reconciled as an artefact of the imaging process due to significantly reduced blood flow. In order to produce sharp images, we employ a Kalman filter to five sequentially obtained images per optical section, since the fluorescence is due to a dextran conjugate in the blood plasma, blood cells themselves do not contribute to the signal. In vessels where blood flow is high, the individual pixel values reflect an average of the varying contributions from both fluorescent and non-fluorescent samples. Since measurements of the same pixel in subsequent frames will also vary, an overall reduction in fluorescence signal may be recorded. The increase in average brightness of the blood vessels can therefore be attributed to a reduction in the contribution of non-fluorescent red blood cells due to loss of

blood flow. This is also supported by the presence, in the later images, of sharp edges within the vessels due to the presence of static red blood cells.

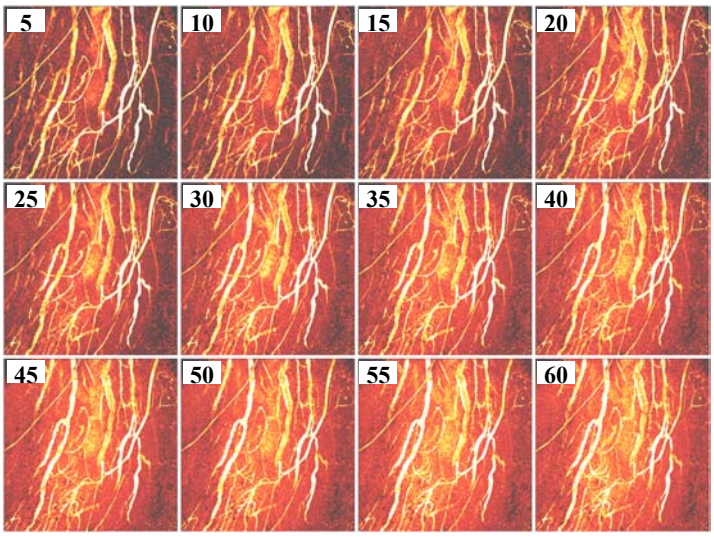

Fig. 3: Extended focus projection of P22 rat tumour vasculature imaged at five minute intervals for up to one hour post administration of CA-4-P. Loss of image contrast due to increased background, indicates extra-vasation of the fluorescent contrast agent due to the vascular damaging effects of CA-4-P.

The effect of extra-vasation of the dextran perfusion marker after administration of CA-4-P is most dramatically observed in fig. 4. Volume rendering of approximately the same region of the tumour (with the same rendering parameters) just prior to, and approximately one hour following, administration of CA-4-P shows a reduction in contrast due to the increase in background signal in the extra-vascular space.

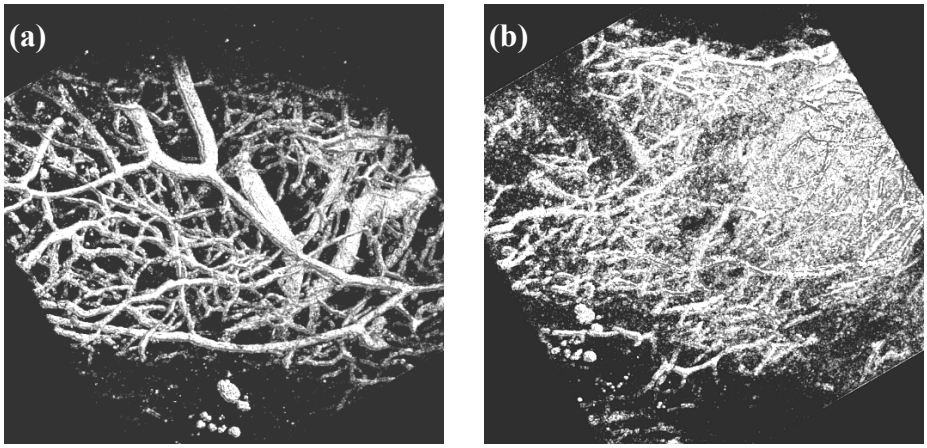

Fig. 4: Volume rendered projections of a region of a P22 rat tumour; a) Prior to administration of CA4-P; b) 1h following intra-peritoneal administration of 30 mg kg^{-1} CA-4-P.

3.4 Blood vessel segmentation by fluorescence lifetime contrast

Multiphoton microscopy has been reported as a method for measurement of angiogenesis in tumours[8], using methods similar to those described here. However, sequential administration (over a period of days) of FITC-dextran can lead to the accumulation of either free FITC (perhaps due to degradation in the liver or by an immune response) or FITC-dextran in the tumour interstitium. Fig. 5 shows a region of a P22 tumour two days after administration of the first bolus of FITC-dextran and a subsequent bolus just prior to imaging to provide the vessel signal. Punctilate staining of individual cells is observed; however, the up-take of the fluorophore appears quite heterogeneous. Presence of such extra-vascular fluorescence reduces contrast for low resolution imaging of the vasculature and whilst segmentation of

the vasculature may be achieved with image processing, information is inevitably lost. In order to improve segmentation at the point of data capture, we have employed fluorescence lifetime as an additional contrast mechanism.

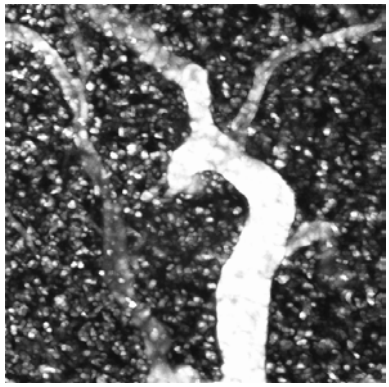

Fig. 5: Region of P22 tumour showing punctilate staining in the tumour bulk due to extra-vasation of the contrast agent on previous days.

An experimental animal with a window chamber was injected with FITC-dextran and imaged conventionally to obtain blood vessel maps on three successive days (with an infusion of contrast agent on each day). During the final experimental session, time-resolved imaging of a single z-plane was undertaken (Fig. 6a) with a total pixel dwell time of ~30 μs. We clearly observed the blood vessels with intensity contrast. However, sequential infusions of the contrast agent have led to accumulation of fluorescent product in the extra-vascular space and in some regions ambiguity in classification of vessels may result (arrows). The fluorescence transient of each pixel was analysed using a single exponential model and the resulting lifetime matrix was segmented using the lifetime histogram (inset) to generate the image in fig. 6b. The fluorescence lifetime matrix reveals that the lifetime of the fluorophore in the vessels is subtly different from that of the extra-vascular space, perhaps indicating a change in the fluorophore environment. Since the steady-state fluorescence indicates some degree of compartmentalisation within the cell population accumulating the fluorophore an increase in the local concentration may lead to self-quenching of the FITC manifested as a decreased average lifetime.

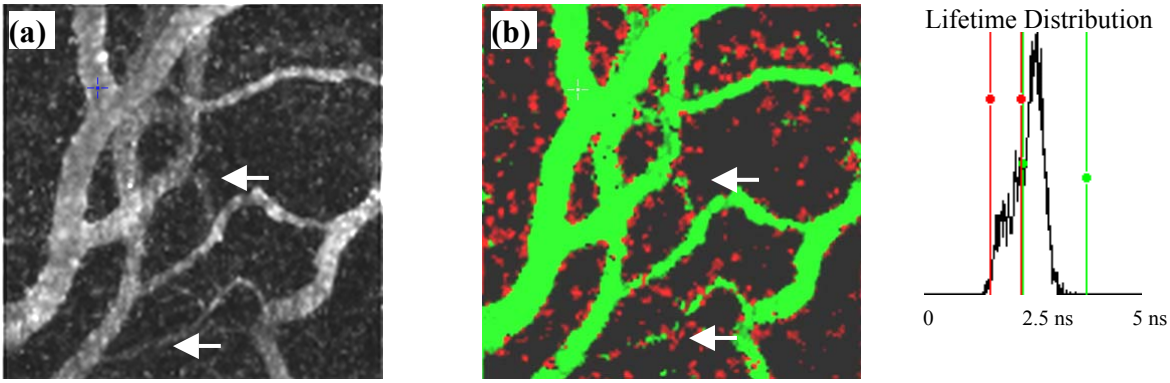

Fig. 6: Blood Vessel Segmentation By Fluorescence Lifetime Contrast Imaging in a BD9 rat bearing a P22 tumour. a) Intensity image: time integrated photon count; b) Segmented lifetime image with vessels clearly delineated.

3.4 Anomolous lifetime contrast in microvascular "permeability" assay.

Measurment of the permeability of the tumour micro-vasculature and diffusion within the extra-vascular space are of key importance if we are to develop predictive models of drug delivery and target interaction. Quantitation of these parameters *in situ* by intravital microscopy has been demonstrated by measurement of the accumulation of fluorescently labeled proteins and/or dextrans in the extravascular space[19]. Multiphoton microscopy was recently shown to be readily adaptable to such measurements of permeability in murine mammary adenocarcinoma within the dorsal skin flap window chamber model by Brown *et al.* in single z-sections in time-lapse mode[8]. In this case tetramethylrhodamine labelled bovine serum albumin (TMR-BSA) was injected and the tumour preparation imaged at

60 s intervals. For comparison of vessel permeability between the McalV model in SCID mice and P22 in BD9 rats and to develop an assay for *in vivo* vessel permeability, we have modified the protocol to use FITC-BSA and to minimise photo-bleaching (since the rate of diffusion into the extravascular space is believed to be relatively slow ($\sim 0.3\text{-}9 \times 10^{-6}$cm s^{-1})), with sequential time-lapse of 300 s for up to 2 hours. A sequence of images from a typical data set is shown in figure 7a. Clear extravasation of the FITC-BSA occurs and the companion graph 7b shows the spatially integrated intensity for region a, normalised to the nearest vessel fluorescence intensity. A diffusion constant is determined from the gradient of a linear fit forced through zero. We make the assumption that the equilibrium time (diffusion within the extravascular matrix) is small in comparison with the vessel permeability.

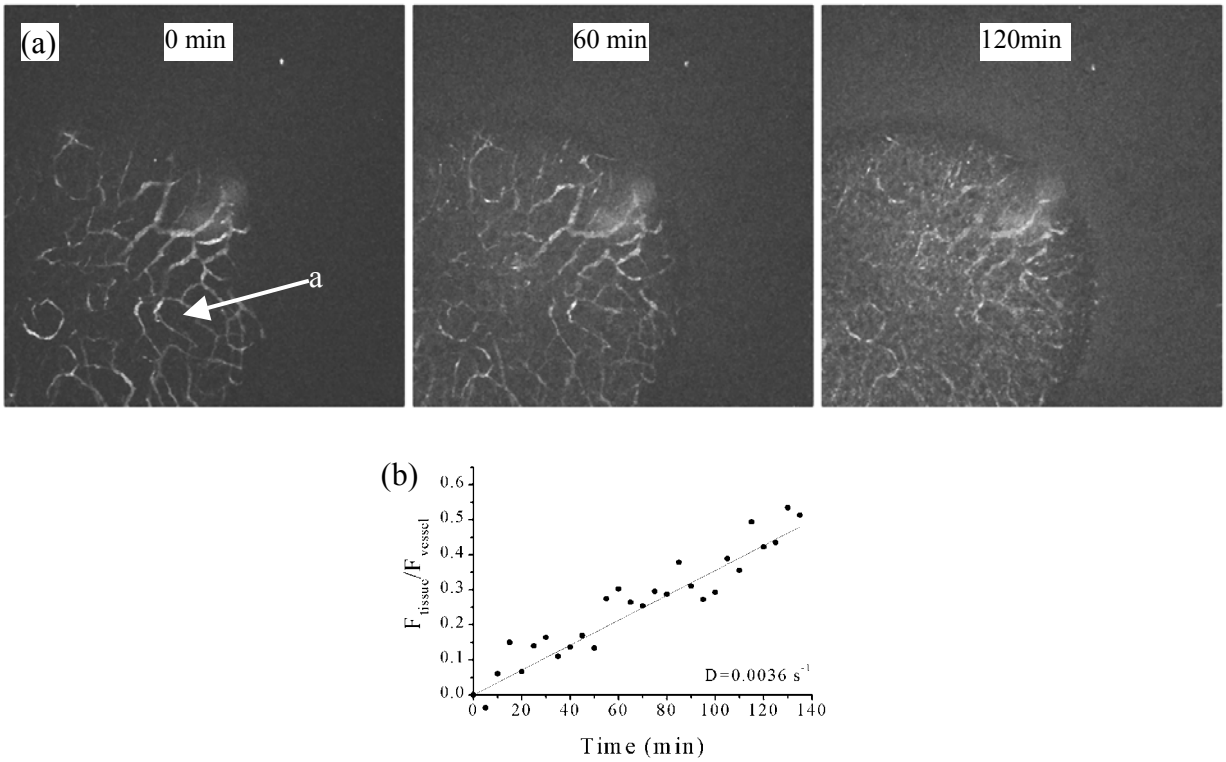

Fig. 7: Typical result from FITC-BSA diffusion experiment for a BD9 rat bearing a P22 tumour; a) Tumour imaged 0, 60, 120 mins after injection of FITC-BSA;. b) Example of normalised diffusion kinetics at region a.

To ensure that the extravascular fluorescence is indeed due to FITC-conjugated albumin and not, for example an increase in autofluorescence, we aquired lifetime imaging data in a single z-plane close to the tumour margin, 200 min after injection of FITC-BSA. A series of ten 30 s acquisitions were accummulated to give sufficient counts in the peak for accurate determination of the kinetics. Figure 8a shows the region of interest as a time-integrated image (photon counts integrated over all time bins). Very little contrast is available to segment the vessels from the tumour bulk in the steady state data. Data analysis in the time-domain reveals biexponetial decay kinetics and unrestrained fits at each pixel reveals excellent contrast between the vessels and the extravascular space (Figure 8b). Closer examination of the individual components of the fit reveals bi-exponential kinetics throughout the probed volume with decay components of 330 ± 40 ps and 3380 ± 280 ps. Contrast in the average lifetime image is principally due to variations in the relative amplitudes of the exponentials (Fig. 9), although there is clear segmentation of the vessels in τ_2. The fast component of the decay appears to be minimally variant throughout the plane and could be indicative of excitation scatter bleedthrough or the presence of endogeneous fluorophores.

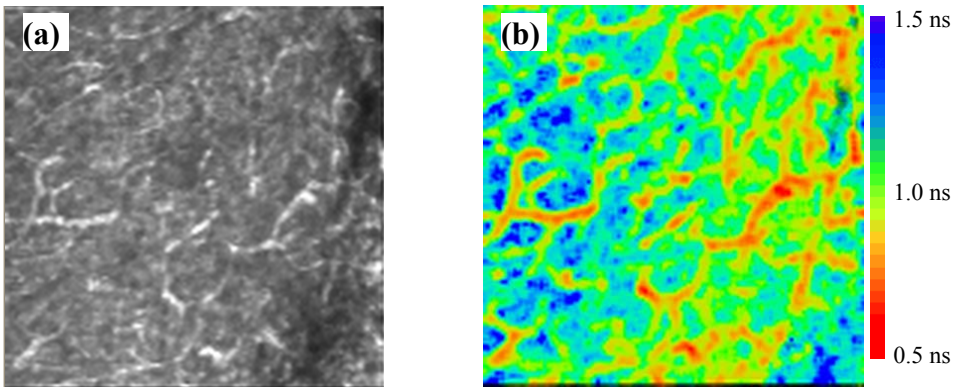

Fig. 8: *In vivo* imaging of FITC-albumin in a BD9 rat bearing a P22 tumour, 1 hour 40 minutes post administration. (a) Intensity Image. (b) Average lifetime image (from $\tau_{av}=(A_1\tau_1+A_2\tau_2)/2$).

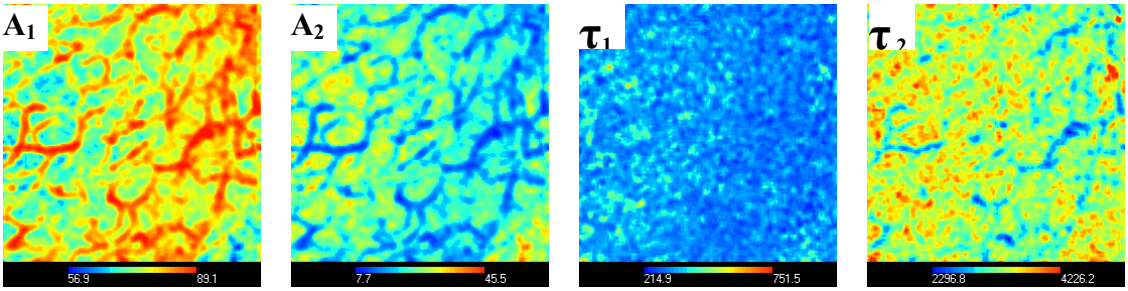

Fig. 9: Individual components of biexponential fit to data in fig. 8.

The presence of contrast between the vasculature and the interstitial space led us to investigate the *ex vivo* behaviour of the FITC-BSA. Table 1 shows the fit parameters for a both a single and bi-exponential decay for FITC-BSA (in acqueous buffer) with data from single pixels in either blood vessels or the extra-vascular space. The measured parameters observed in buffer solution show differences to both those observed for the lumen of the blood vessels and the extra-vascular space, indicating that significant modification of the probe complex occurs *in vivo*. These data are consistent with the hypothesis that the conjugated FITC molecules are experiencing self-quenching in the excited state. This is supported by comparison with a second FITC-BSA (molecular probes) sample with a lower molar conjugation ratio and unconjugated FITC data (also shown).

Table 1: Fit parameters for FITC-BSA

Preparation	τ_1	τ_2	A_1	A_2	χ^2
FITC-BSA buffer (12:1 molar ratio)	668 280	1438	1 0.89	0.11	5.26 2.97
FITC-BSA buffer (6:1 molar ratio)	2130 510	2750	1 51	49	7.55 1.48
FITC-unconjugated	3680		1		1.29
FITC-BSA tissue	2347 406	3575	1 0.67	0.33	9.80 2.85
FITC-BSA vessel	1080 292	2364	1 0.90	0.10	9.55 2.19
FITC-BSA digested <10kD	3042 379	3253	1 0.15	0.85	1.30 1.22
10 kD< FITC-BSA digested <30kD	2818 373	3024	1 0.25	0.75	3.03 1.57
FITC-BSA digested >30kD	1736 311	2771	0.74	0.26	6.64 2.70

The observed increase in τ_2 for the *in vivo* data, lead us to suggest that the FITC-BSA may be unquenching due to either conformational change (unravelling or denaturing of the protein) or the removal of FITC molecules by biochemical

processing. We examined the possibility of unquenching due to unravelling the protein and cleaving of FITC-bound peptides by incubation of FITC-BSA with trypsin (0.1 % w/v) for a period of 10 mins with kinetics observed at 30 s intervals. Enzymatic action of the trypsin leads to unquenching of the slow component of the decay (fig. 10b) but no significant change in the fast (sub ns) decay (fig.10a), we also observe modification of the ratio of A_2/A_1 consistent with the unquenching of FITC (fig. 10c). Separation of the resulting solution with the reaction at completion (circa. 2hours) was undertaken with micro-sieves (Millipore Ltd) in an ultracentrifuge. The decay kinetics for a < 3kD, the >30 kD fractions and those in the mass range >10 kD but <30 kD, are given in table 1. Kinetics for the <10 kD fraction are consistent with those observed for free FITC, indicating that whilst the fluorochrome may still be bound to a peptide group, the local concentration of FITC is not sufficient to quench the lifetime. The >30 kD fraction is also consistent with an unquenching hypothesis, since the degree of quenching as a function of time (Fig. 10d) reflects a reduction in local concentration of fluorophores/quenchers.

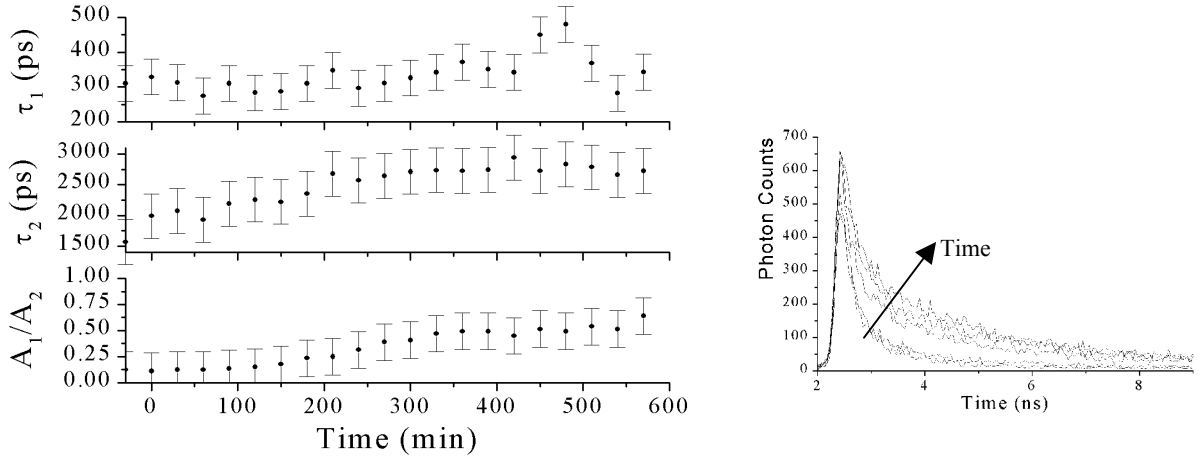

Fig. 10: Time-course of trypsin modification of FITC-BSA kinetics; a) τ_1; b) τ_2; c) A_2/A_1; d) Kinetics as a function of time

Unquenching of the FITC-BSA either due to the unravelling of the protein or the sequencial concatenation of the peptides gives a self-consistent hypothesis which we can examine *in vivo*. Sequential blood samples were collected from three BD9 rats (without tumour) to test the hypothesis. The blood was subsequently spun down to remove RBC and then separated into <30KD and >30kD fractions by ultracentrafuge (as previously). Fluorescence kinetics were measured at room temperature in small capillaries and the steady state emission also measured for both fractions at a 100 min time point (data not shown), these data are summarised in Fig.11. We observe an increase in τ_2 which is consistent with the concatenation of FITC-BSA by trypsin digestion observed in fig. 10 and Table 1. The observed reduction in τ_1, is almost certainly a fitting error and these data may benefit from global analysis. Steady-state fluorescence measurements reveal that the fluorescence due to <10kD species at the 100 min time point is comparable to that of the parent compound. We also observe variation in both the absorption and emission spectra consistant with unquenching (data not shown). Whilst the relative concentration of free FITC may be low in comparison to the parent FITC-BSA form, clearly the increase in fluorescence intensity due to unquenching will have a marked effect. Selection of FITC-BSA with a reduced conjugation ratio may minimise the relative contribution of deconcatenated species in the diffusion assay.

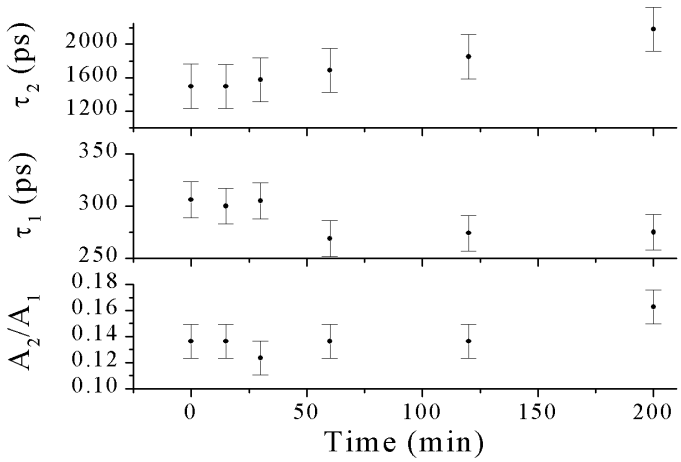

Fig. 11 FITC-BSA Blood fraction fluorescence measurement: Variation in fitting parameters for time domain fluorescence of filtered >30 kD blood fraction.

These data suggest that the anomolous fluorescence lifetime contrast observed for *in vivo* experiments for FITC-BSA are due to the unquenching of the FITC chromophore as a function of time. Observations of concatenation of the FITC-BSA by digestion in trypsin suggest a possible mechanism for unquenching and this is confirmed in the extraction of blood fractions from rodents without tumours as a function of time post-administration. Examination of tissue from the liver and spleen suggests these are the primary sites for modification of FITC-BSA (data not shown). Possible explanations for the modification are beyond the scope of this paper but may involve the antigen regulatory function of these tissues. Similar fluorescence lifetime unquenching has been observed for macrophage modulated antigen processing of FITC-BSA[20]. These results imply that the measurement of FITC-BSA extravasation is unlikely to provide an accurrate determination of vascular permeability or interstitial diffusion parameters without precise knowledge of the species involved. Accumulation of low molecular weight species in the interstitial space in extravasation assays of FITC-BSA may be responsible for much of the fluorescence observed due to the decreased hydrodynamic radius and increased quantum efficiency of the complex compared to the FITC-BSA parent species. Accumulation would, in this instance, follow the time-integrated concentration of the degraded/deconcatenated species. With sufficient investigation and modelling, it may be possible to extract the permeability constant of the vessel walls due to FITC-BSA based on relative concentration of low and high molecular weight species or from observed kinetics. However, such measurements will be subject to considerable uncertainty even in comparative studies.

4. CONCLUSIONS

We have shown that blood vessel architecture may be determined from *in vivo* tumour models by multiphoton microscopy. Manual segmentation of the vascular architecture is possible from the data and statistical parameters describing the tumour may be extracted. Segmentation of the FITC-dextran labeled vasculature in the presence of compartmentalised FITC-dextran in the extravascular space has been performed by fluorescence lifetime imaging. Anomolous fluorescence lifetime contrast in measurements of the extravasation of FITC-BSA has been investigated and found unquenching of the FITC fluorescence as the BSA is deconcatenated principally by enzymatic action in the liver. Our results suggest that the interpretation of permeability data from steady-state MPM should take into account the metabolism of the sensor molecule in the liver. Certainly these results warrant a careful re-evaluation of fluorescently labelled BSA for permeability assays *in vivo*.

ACKNOWLEDGEMENTS

This work was supported by the Cancer Research Campaign and by the Royal Society Paul Instrument Fund. We thank Oxigene Ltd for supplying Combretastatin A4-P.

REFERENCES

[1] M.K. Reed (Ed), "Commercial applications of ultrafast lasers," *Proc. SPIE.* **3269**, 1998.
[2] W. Denk, J.H. Strickler and W. W. Webb, "Two-photon laser scanning fluorescence microscopy," *Science* **248**, pp. 73-76, 1990.
[3] D.R. Sandison, D.W. Piston, R. M. Williams and W. W. Webb, "Quantitative comparison of background rejection, signal-to-noise ratio and resolution in confocal and full field laser scanning microscopes," *Appl. Opt.* **34**, pp. 3576-3588, 1995.
[4] W. Denk and K. Svoboda, *"Photon upmanship: Why multiphoton imaging is more than just a gimmick," Neuron* **18**, pp. 351-357, 1997.
[5] J. M. Squirrell, D. L. Wokosin, J. G. White and B. D. Bavister, "Long term two-photon fluorescence imaging of mammalian embryos without compromising viability," *Nature: Biotechnology* **17**, pp. 763-767, 1999.
[6] B. R. Masters, P. T. C. So, and E. Gratton, "Optical biopsy of in vivo human skin: multiphoton excitation microscopy," *Lasers Med. Sci.* **13**, pp. 196-203, 1998.
[7] D. W. Piston, B.R. Masters and W. W. Webb, "Three dimensionally resolved NAD(P)H cellular metabolic redox imaging of the in situ cornea with two-photon excitation laser scanning microscopy," *J. Microscopy* **178**(1), pp 20-27, 1995.
[8] E. B. Brown, R. B. Cambell, Y. Tsuzuki , L. Xu, P. Carmeliet, D. Fukumura and R. K. Jain, "*In vivo* measurement of gene expression, angiogenesis and physiological function in tumours using multiphoton laser scanning microscopy," *Nature Medicine* **7**, pp864-868, 2001.
[9] D. Kleinfeld, P. P. Mitra, F. Helmchen, W. Denk, "Fluctuations and stimulus induced changes in blood flow observed in individual capillaries in layers 1 through 4 of rat neocortex," *Proc. Nat. Acad. Sci*. USA **95**, pp15741-15746, 1998.
[10] Thomlinson and Gray, "The histological structure of some human lung cancers and the possible implications for radiotherapy", Br. *J. Cancer* **9**, pp 539-549, 1955.
[11] C. M. L. West, R. A. Cooper, J. Loncaster, D. P. Wilks and M. Bromley, "Tumour vascularity: A histological measure of angiogenesis and hypoxia," *Cancer Res*. **61**, pp2907-2910, 2001.
[12] G. D. Dark, S. A. Hills, V. E. Prise, G. M. Tozer, G. R. Pettit and D. J. Chaplin, "Combretastatin A4, an agent that displays potent and selective toxicity toward tumour vasculature," Cancer Res. **57**, pp. 1829-1834, 1997.
[13] E. B. Brown, R. B. Campbell, Y. Tsuzuki, D. Fukumura and R. K. Jain, "Measurement of physiological parameters in tumors in vivo using MPLSM." *Proc. SPIE* **4262**, pp. 134-145, 2001.
[14] J. S. Cordeelis, J. Wyckoff and J. E. Segall, "Imaging of cancer invasion and metastisis using green fluorescent protein." *Euro. J. Cancer* **36**, pp1671-1680, 2000.
[15] W. Becker, A. Bergmann, K. Konig and U. Tirlapur, "Picosecond fluorescence lifetime microscopy by TCSPC imaging," *Proc. SPIE* **4262**, pp414-419, 2001.
[16] H. D. Papenfuss, J. F. Gross, M. Intaglietta and F. A. Treese, "A transparent access chamber for the rat dorsal skin fold," *Microvasc. Res*. **18,** pp. 311-318, 1979.
[17] M. W. Dewhirst, C. Gustafson, J. F. Gross, and C. Y. Tso, "Temporal effects of 5.0 Gy radiation in healing subcutaneous micro-vasculature of a dorsal flap window chamber," *Rad. Res.* **112,** pp. 581-591, 1987.
[18] G. M. Tozer & K. M. Shaffi, "Modification of tumour blood flow using the hypertensive agent, angiotensin II," *Br. J. Cancer* **67,** pp 981-988, 1993.
[19] R. H. Adamson, J. F. Lenz and F. E. Curry, "Quantitative laser scanning confocal microscopy on single capillaries: Permeability measurement," *Microcirculation* **1**(4), pp. 251-265, 1994.
[20] T. French, P. T. So, D. J. Weaver Jr, T. Coelho-Sampaio, E. Gratton, E. W. Voss Jr, J. Carrero "Two-photon fluorescence lifetime imaging microscopy of macrophage-mediated antigen processing." *J. Microscopy* **185**(3), pp339-353, 1997.